Computer Physics Communications 270 (2022) 108179

Contents lists available at ScienceDirect

Computer Physics Communications

www.elsevier.com/locate/cpc

FourPhonon: An extension module to ShengBTE for computing four-phonon scattering rates and thermal conductivity ☆,☆☆

Zherui Han [a], Xiaolong Yang [b,c], Wu Li [c], Tianli Feng [d], Xiulin Ruan [a,*]

[a] School of Mechanical Engineering and the Birck Nanotechnology Center, Purdue University, West Lafayette, IN 47907-2088, USA
[b] College of Physics, and Center of Quantum Materials and Devices, Chongqing University, Chongqing 401331, China
[c] Institute for Advanced Study, Shenzhen University, Nanhai Avenue 3688, Shenzhen 518060, China
[d] Department of Mechanical Engineering, University of Utah, Salt Lake City, UT 84112, USA

ARTICLE INFO

Article history:
Received 10 April 2021
Received in revised form 9 August 2021
Accepted 4 September 2021
Available online 28 September 2021

Keywords:
Thermal conductivity prediction
Four-phonon scattering
Boltzmann transport equation
First principles
Density functional theory

ABSTRACT

`FourPhonon` is a computational package that can calculate four-phonon scattering rates in crystals. It is built within `ShengBTE` framework, which is a well-recognized lattice thermal conductivity solver based on Boltzmann transport equation. An adaptive energy broadening scheme is implemented for the calculation of four-phonon scattering rates. In analogy with `thirdorder.py` in `ShengBTE`, we also provide a separate python script, `Fourthorder.py`, to calculate fourth-order interatomic force constants. The extension module preserves all the nice features of the well-recognized lattice thermal conductivity solver `ShengBTE`, including good parallelism and straightforward workflow. In this paper, we discuss the general theory, program design, and example calculations on Si, BAs and $LiCoO_2$.

Program summary
Program Title: `FourPhonon`
CPC Library link to program files: https://doi.org/10.17632/jjcwt5436h.1
Developer's repository link: https://github.com/FourPhonon
Licensing provisions: GNU General Public License version 3
Programming language: Fortran 90, MPI
Nature of problem: Calculation of lattice thermal conductivity and related quantities, determination of both three-phonon and four-phonon scattering rates
Solution method: Four-phonon scattering rates at RTA level, adaptive broadening scheme
Additional comments including restrictions and unusual features: For a productive run, one needs to use High Performance Computing facilities and it takes several hours to several days to finish calculations

1. Introduction

Phonons, quantum mechanical description of atomic vibrations in crystals, are the main heat carriers in most insulators, semiconductors and some semimetals. Phonon properties and lattice thermal conductivity are largely determined by phonon-phonon interactions. Starting from 1929 [1] when Peierls proposed the first formulation to calculate thermal conductivity using Boltzmann transport equation (BTE), subsequent models [2–5] with fewer fitting parameters have emerged owing to the advancement of both theory and computational power. About a decade ago, Broido et al. [6] combined first-principles calculations and phonon Boltzmann transport equation, and enabled first-principles prediction of thermal conductivity. This method has gained great success in predicting thermal properties, and not until recently the common practice was to consider phonon-phonon interactions up to the lowest order, i.e., three-phonon scattering [7–11].

☆ The review of this paper was arranged by Prof. W. Martin.
☆☆ This paper and its associated computer program are available via the Computer Physics Communications homepage on ScienceDirect (http://www.sciencedirect.com/science/journal/00104655).
* Corresponding author.
E-mail address: ruan@purdue.edu (X. Ruan).

https://doi.org/10.1016/j.cpc.2021.108179
0010-4655/

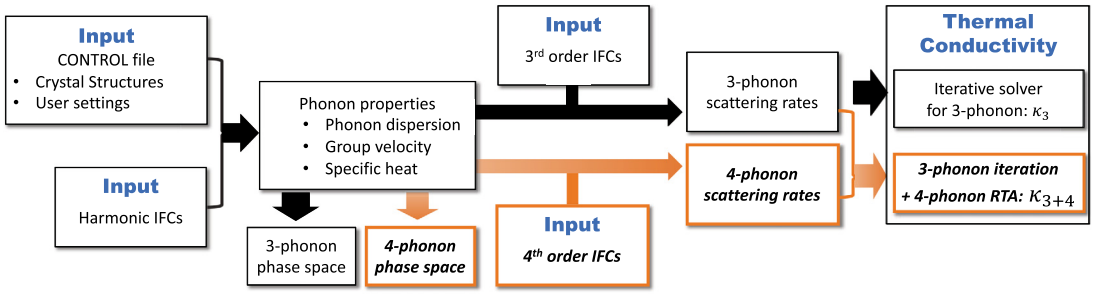

Fig. 1. Modified workflow of `ShengBTE` + `FourPhonon`. Orange parts represent added modules by `FourPhonon`. (For interpretation of the colors in the figure(s), the reader is referred to the web version of this article.)

Among various computational tools for calculating the lattice thermal conductivity, `ShengBTE` [12] is a well-developed and mostly used software package.

Phonon-phonon interactions stem from the intrinsic lattice anharmonicity of materials. While three-phonon scattering was assumed to be adequate in describing anharmonicity [6–8], Feng and Ruan developed a rigorous four-phonon scattering formalism in 2016 [13], and revealed that higher-order anharmonicity can play a significant role. In 2017, Feng, Lindsay, and Ruan predicted that four-phonon scattering is surprisingly strong in BAs [14], a material predicted to possess higher thermal conductivity than diamond by three-phonon scattering theory [8]. In 2018, three independent experiments [15–17] confirmed the significance of four-phonon scattering in BAs. Subsequent studies pursuing four-phonon effect have proved its importance in a broader range of systems [18–23], including insulators, semiconductors and semimetals with topics covering thermal conductivity predictions, radiative properties, and phonon linewidths. Future research into material properties at high temperatures, optical phonon energy decay, infrared properties or other interesting topics may require to include four-phonon scattering as well. A detailed discussion can be found in Ref. [24]. Despite the evident importance of four-phonon scattering calculations, they have remained largely inaccessible to the thermal transport community due to the complex form and large computational load. To the best of our knowledge, there is not an open-source software available yet to perform four-phonon calculations and the newly developed tool presented in this paper should be beneficial.

Here, we present a computational package for four-phonon scattering calculations, `FourPhonon`. We develop this tool as an extension module to `ShengBTE`, which has good extensibility. With a subroutine `Fourthorder.py` to calculate fourth-order interatomic force constants (IFCs) through first principles, `FourPhonon` is capable of computing four-phonon phase space, scattering rates from both normal and Umklapp processes, and lattice thermal conductivity. Its operation is fully compatible with the current `ShengBTE` package.

The remainder of this paper is organized as follows. Section 2 presents the theoretical background and computational details of the `FourPhonon` package. In Section 3, we show three case studies on representative materials: Si, BAs and $LiCoO_2$. We also document the input and output files of our software in Appendix A.

2. Methodology and computational details

2.1. *ShengBTE + FourPhonon workflow*

`FourPhonon` is built within `ShengBTE` framework and its execution is fully compatible with `ShengBTE`. Before explaining `FourPhonon`, we briefly review the basic `ShengBTE` workflow [12]. It uses second-order and third-order force constants as inputs, retrieves phonon properties from harmonic calculations, estimates the available three-phonon scattering phase space, and then calculates the three-phonon scattering rates and lattice thermal conductivity. Besides the 2^{nd}- and 3^{rd}-order force constants files, users need to provide another input file, named `CONTROL`, which contains all the user-specified settings and parameters, including crystal structural information, temperature, **q**-mesh, broadening factor, etc. On the basis of this workflow, `FourPhonon` requires an additional input file with fourth-order force constants. Flag is also added to the `CONTROL` file to enable `FourPhonon` utilities, namely `four_phonon`. When combined with other inherent flags or settings, users can perform various tasks, gaining insight into four-phonon scattering. We now illustrate the modified workflow in more details. A workflow chart is presented in Fig. 1.

Due to the great computational cost of four-phonon scattering in most materials, one may need to estimate first how significant four-phonon scattering is compared to three-phonon scattering in a certain system. One can use the available three-phonon and four-phonon phase spaces as a criterion. To calculate these values, users can turn on the flags `onlyharmonic` and `four_phonon`, which will count the number of four-phonon scattering processes so that one can have a quick estimation of the computational demand when going forward.

Another particular problem is that one may need to determine whether to solve the BTE exactly with an iterative scheme beyond single mode relaxation time approximation (SMRTA, or RTA) to get converged thermal conductivity. Some theoretical works have indicated that this is closely related to the relative strength of phonon normal/Umklapp processes [18,25]. Since the iterative scheme would require huge computational resources (both processors and memory), users can first perform calculations in SMRTA scheme by turning on `four_phonon` flag and disable `convergence` flag. SMRTA calculations usually take much less time to finish than iterative scheme and would output scattering rates from normal/Umklapp scattering events separately. If Umklapp processes are dominant, then the accuracy in thermal conductivity may be acceptable without further utilizing iterative scheme. If normal processes are relatively strong, one can apply the iterative scheme to BTE up to three-phonon scattering by turning on `convergence` flag, with four-phonon scattering rates treated at the RTA level. Presently, this package is not able to involve the four-phonon scattering phase space in the iteration scheme due to the exceptionally high memory demands. Further optimization could be made to include this functionality in the future.

2.2. Implemented four-phonon formalism

The linearized phonon Boltzmann transport equation with three-phonon scattering has been extensively studied in the literature, and the formalism on four-phonon scattering has also been well documented in several preceding papers [13,14,18]. Here, we only introduce a unified formalism implemented in our program and make all the corresponding notations consistent with the one used in `ShengBTE` [12]. At steady state, the rate of change of phonon distribution function due to diffusion and scattering should be balanced out for a certain phonon mode λ:

$$\frac{\partial n_\lambda}{\partial t} = \left.\frac{\partial n_\lambda}{\partial t}\right|_{\text{diff}} + \left.\frac{\partial n_\lambda}{\partial t}\right|_{\text{scatt}} \equiv 0. \tag{1}$$

Using the relaxation time approximation, the scattering term is expressed as:

$$\left.\frac{\partial n_\lambda}{\partial t}\right|_{\text{scatt}} = \frac{n_\lambda - n_\lambda^0}{\tau_\lambda}, \tag{2}$$

where n_λ^0 and τ_λ are the equilibrium Bose-Einstein distribution and the relaxation time for phonon mode λ. The diffusion term is $\left.\frac{\partial n_\lambda}{\partial t}\right|_{\text{diff}} = -\frac{\partial n_\lambda}{\partial T}\nabla T \cdot \mathbf{v}_\lambda$ with $\mathbf{v}_\lambda$ being the group velocity. It is convenient to write the equation in terms of the deviation from n_λ^0 as $n_\lambda = n_\lambda^0 - \mathbf{F}_\lambda \cdot \frac{\partial n_\lambda}{\partial T}\nabla T - \ldots$, and only keep the linear terms with $\mathbf{F}_\lambda$ in the scattering term.

Then, for a certain mode λ, the linearized BTE [5] is expressed as:

$$\mathbf{F}_\lambda = \tau_\lambda^0(\mathbf{v}_\lambda + \mathbf{\Delta}_\lambda), \tag{3}$$

where τ_λ^0 is the relaxation time for mode λ under SMRTA. $\mathbf{\Delta}_\lambda$ works for iterative scheme and is a quantity showing the phonon population deviation from SMRTA scheme. With the inclusion of four-phonon scattering, $\mathbf{\Delta}_\lambda$ and τ_λ^0 (0 represents zeroth-order in iterations) are computed as:

$$\begin{aligned}
\mathbf{\Delta}_\lambda =& \frac{1}{N}\sum_{\lambda'\lambda''}^{(+)} \Gamma^{(+)}_{\lambda\lambda'\lambda''}(\xi_{\lambda\lambda''}\mathbf{F}_{\lambda''} - \xi_{\lambda\lambda'}\mathbf{F}_{\lambda'}) + \frac{1}{N}\sum_{\lambda'\lambda''}^{(-)} \frac{1}{2}\Gamma^{(-)}_{\lambda\lambda'\lambda''}(\xi_{\lambda\lambda''}\mathbf{F}_{\lambda''} + \xi_{\lambda\lambda'}\mathbf{F}_{\lambda'}) \\
&\left.\begin{aligned}
&+\frac{1}{N}\sum_{\lambda'\lambda''\lambda'''}^{(++)} \frac{1}{2}\Gamma^{(++)}_{\lambda\lambda'\lambda''\lambda'''}(\xi_{\lambda\lambda'''}\mathbf{F}_{\lambda'''} - \xi_{\lambda\lambda'}\mathbf{F}_{\lambda'} - \xi_{\lambda\lambda''}\mathbf{F}_{\lambda''}) \\
&+\frac{1}{N}\sum_{\lambda'\lambda''\lambda'''}^{(+-)} \frac{1}{2}\Gamma^{(+-)}_{\lambda\lambda'\lambda''\lambda'''}(\xi_{\lambda\lambda'''}\mathbf{F}_{\lambda'''} - \xi_{\lambda\lambda'}\mathbf{F}_{\lambda'} + \xi_{\lambda\lambda''}\mathbf{F}_{\lambda''}) \\
&+\frac{1}{N}\sum_{\lambda'\lambda''\lambda'''}^{(--)} \frac{1}{6}\Gamma^{(--)}_{\lambda\lambda'\lambda''\lambda'''}(\xi_{\lambda\lambda'''}\mathbf{F}_{\lambda'''} + \xi_{\lambda\lambda'}\mathbf{F}_{\lambda'} + \xi_{\lambda\lambda''}\mathbf{F}_{\lambda''})
\end{aligned}\right\} \text{four-phonon terms} \\
&+\frac{1}{N}\sum_{\lambda'}^{(\text{iso})} \Gamma^{(\text{iso})}_{\lambda\lambda'}\xi_{\lambda\lambda'}\mathbf{F}_{\lambda'},
\end{aligned} \tag{4}$$

$$\begin{aligned}
\frac{1}{\tau_\lambda^0} =& \frac{1}{N}\left(\sum_{\lambda'\lambda''}^{(+)} \Gamma^{(+)}_{\lambda\lambda'\lambda''} + \sum_{\lambda'\lambda''}^{(-)} \frac{1}{2}\Gamma^{(-)}_{\lambda\lambda'\lambda''}\right) + \frac{1}{N}\sum_{\lambda'}^{(\text{iso})} \Gamma^{(\text{iso})}_{\lambda\lambda'} \\
&\underbrace{+\frac{1}{N}\left(\sum_{\lambda'\lambda''\lambda'''}^{(++)} \frac{1}{2}\Gamma^{(++)}_{\lambda\lambda'\lambda''\lambda'''} + \sum_{\lambda'\lambda''\lambda'''}^{(+-)} \frac{1}{2}\Gamma^{(+-)}_{\lambda\lambda'\lambda''\lambda'''} + \sum_{\lambda'\lambda''\lambda'''}^{(--)} \frac{1}{6}\Gamma^{(--)}_{\lambda\lambda'\lambda''\lambda'''}\right)}_{\text{four-phonon scattering terms}},
\end{aligned} \tag{5}$$

where N is the total grid of $\mathbf{q}$ points. $\xi_{\lambda\lambda'} = \omega_{\lambda'}/\omega_{\lambda''}$. The superscripts $(\pm)$ or $(\pm\pm)$ represent the three-phonon (3ph) and four-phonon (4ph) processes, namely $\mathbf{q}'' = \mathbf{q} \pm \mathbf{q}' + \mathbf{Q}$ and $\mathbf{q}''' = \mathbf{q} \pm \mathbf{q}' \pm \mathbf{q}'' + \mathbf{Q}$, respectively. $\mathbf{Q}$ is a reciprocal lattice vector with $\mathbf{Q} = 0$ implying normal process. Note that Eq. (4) is the full expression for three- and four-phonon iterative scheme, whereas the current version of `FourPhonon` does not support such functionality and excludes the four-phonon terms in Eq. (4). $\Gamma^{(\text{iso})}$ is the isotope scattering rates. Other Γ with superscripts denote the scattering rates for 3ph and 4ph processes, and are computed by scattering probability matrices [13,26]:

$$\begin{aligned}
\Gamma^{(+)}_{\lambda\lambda'\lambda''} &= \frac{\hbar\pi}{4}\frac{n^0_{\lambda'} - n^0_{\lambda''}}{\omega_\lambda\omega_{\lambda'}\omega_{\lambda''}}|V^{(+)}_{\lambda\lambda'\lambda''}|^2\delta(\omega_\lambda + \omega_{\lambda'} - \omega_{\lambda''}) \\
\Gamma^{(-)}_{\lambda\lambda'\lambda''} &= \frac{\hbar\pi}{4}\frac{n^0_{\lambda'} + n^0_{\lambda''} + 1}{\omega_\lambda\omega_{\lambda'}\omega_{\lambda''}}|V^{(-)}_{\lambda\lambda'\lambda''}|^2\delta(\omega_\lambda - \omega_{\lambda'} - \omega_{\lambda''}),
\end{aligned} \tag{6}$$

$$\Gamma^{(++)}_{\lambda\lambda'\lambda''\lambda'''} = \frac{\hbar^2\pi}{8N}\frac{(1+n^0_{\lambda'})(1+n^0_{\lambda''})n^0_{\lambda'''}}{n^0_\lambda}|V^{(++)}_{\lambda\lambda'\lambda''\lambda'''}|^2\frac{\delta(\omega_\lambda+\omega_{\lambda'}+\omega_{\lambda''}-\omega_{\lambda'''})}{\omega_\lambda\omega_{\lambda'}\omega_{\lambda''}\omega_{\lambda'''}}$$
$$\Gamma^{(+-)}_{\lambda\lambda'\lambda''\lambda'''} = \frac{\hbar^2\pi}{8N}\frac{(1+n^0_{\lambda'})n^0_{\lambda''}n^0_{\lambda'''}}{n^0_\lambda}|V^{(+-)}_{\lambda\lambda'\lambda''\lambda'''}|^2\frac{\delta(\omega_\lambda+\omega_{\lambda'}-\omega_{\lambda''}-\omega_{\lambda'''})}{\omega_\lambda\omega_{\lambda'}\omega_{\lambda''}\omega_{\lambda'''}} \tag{7}$$
$$\Gamma^{(--)}_{\lambda\lambda'\lambda''\lambda'''} = \frac{\hbar^2\pi}{8N}\frac{n^0_{\lambda'}n^0_{\lambda''}n^0_{\lambda'''}}{n^0_\lambda}|V^{(--)}_{\lambda\lambda'\lambda''\lambda'''}|^2\frac{\delta(\omega_\lambda-\omega_{\lambda'}-\omega_{\lambda''}-\omega_{\lambda'''})}{\omega_\lambda\omega_{\lambda'}\omega_{\lambda''}\omega_{\lambda'''}},$$

where Eq. (6) is for three-phonon processes and Eq. (7) for four-phonon processes, with n^0_λ being the phonon Bose-Einstein distribution at equilibrium, ω_λ being the phonon frequency for a certain mode λ. Conservation of energy is enforced by the Dirac delta function δ. In Eq. (6) and (7), the matrix elements V are given by the Fourier transformation of force constants, or transition probability matrices:

$$V^{(\pm)}_{\lambda\lambda'\lambda''} = \sum_{ijk}\sum_{\alpha\beta\gamma}\Phi^{\alpha\beta\gamma}_{ijk}\frac{e^\lambda_\alpha(i)e^{\pm\lambda'}_\beta(j)e^{-\lambda''}_\gamma(k)}{\sqrt{\bar{M}_i\bar{M}_j\bar{M}_k}}e^{\pm i\mathbf{q}'\cdot\mathbf{r}_j}e^{-i\mathbf{q}''\cdot\mathbf{r}_k}, \tag{8}$$

$$V^{(\pm\pm)}_{\lambda\lambda'\lambda''\lambda'''} = \sum_{ijkl}\sum_{\alpha\beta\gamma\theta}\Phi^{\alpha\beta\gamma\theta}_{ijkl}\frac{e^\lambda_\alpha(i)e^{\pm\lambda'}_\beta(j)e^{\pm\lambda''}_\gamma(k)e^{-\lambda'''}_\theta(l)}{\sqrt{\bar{M}_i\bar{M}_j\bar{M}_k\bar{M}_l}}e^{\pm i\mathbf{q}'\cdot\mathbf{r}_j}e^{\pm i\mathbf{q}''\cdot\mathbf{r}_k}e^{-i\mathbf{q}'''\cdot\mathbf{r}_l}, \tag{9}$$

where i, j, k, l denote the atomic indices and $\alpha, \beta, \gamma, \theta$ denote the Cartesian dimensions x, y, or z. $\Phi^{\alpha\beta\gamma}_{ijk}$ and $\Phi^{\alpha\beta\gamma\theta}_{ijkl}$ are the third-order and fourth-order force constants, respectively. $e^\lambda_\alpha(i)$ is the eigenvector component for a mode. $\mathbf{r}_j$ is the position vector of the unit cell where j-th atom lies, and M_j is its mass.

The remaining formulae including the isotope scattering and the expression of thermal conductivity are the same as `ShengBTE`, so are not elaborated in this paper.

2.3. Fourth-order force constants

The potential energy of crystals can be written as a Taylor expansion with respect to the atomic displacement based on perturbation theory [26]

$$E = E_0 + \frac{1}{2}\sum_{\substack{ij\\\alpha\beta}}\Phi^{\alpha\beta}_{ij}r^\alpha_i r^\beta_j + \frac{1}{3!}\sum_{\substack{ijk\\\alpha\beta\gamma}}\Phi^{\alpha\beta\gamma}_{ijk}r^\alpha_i r^\beta_j r^\gamma_k + \frac{1}{4!}\sum_{\substack{ijkl\\\alpha\beta\gamma\theta}}\Phi^{\alpha\beta\gamma\theta}_{ijkl}r^\alpha_i r^\beta_j r^\gamma_k r^\theta_l + \ldots, \tag{10}$$

where r^α_i is the displacement of atom i along the $\alpha(x, y, z)$ direction, E_0 is the potential energy when $r = 0$, and the coefficients Φ in the n-th order term are the corresponding n-th order interatomic force constants (IFCs). Given by the translational symmetry, fourth-order IFCs depend only on the relative coordinates of atom quartette (i, j, k, l) rather than the absolute coordinates of the four atoms. The IFCs are usually determined by either a finite-difference scheme on the atomic forces [12] or fitting the atomic displacement-force relations [27].

In `Fourthorder.py` we employ a real-space finite-difference method to calculate the fourth-order IFCs:

$$\begin{aligned}
\Phi^{\alpha\beta\gamma\theta}_{ijkl} =& \frac{\partial^4 E}{\partial r^\alpha_i\partial r^\beta_j\partial r^\gamma_k\partial r^\theta_l}\\
\approx& \frac{1}{2h}\left[\frac{\partial^3 E}{\partial r^\beta_j\partial r^\gamma_k\partial r^\theta_l}(r^\alpha_i=h) - \frac{\partial^3 E}{\partial r^\beta_j\partial r^\gamma_k\partial r^\theta_l}(r^\alpha_i=-h)\right]\\
\approx& \frac{1}{4h^2}\left[\frac{\partial^2 E}{\partial r^\gamma_k\partial r^\theta_l}(r^\alpha_i=h, r^\beta_j=h) - \frac{\partial^2 E}{\partial r^\gamma_k\partial r^\theta_l}(r^\alpha_i=h, r^\beta_j=-h)\right.\\
&\left. - \frac{\partial^2 E}{\partial r^\gamma_k\partial r^\theta_l}(r^\alpha_i=-h, r^\beta_j=h) + \frac{\partial^2 E}{\partial r^\gamma_k\partial r^\theta_l}(r^\alpha_i=-h, r^\beta_j=-h)\right]\\
\approx& \frac{1}{8h^3}\Big[F^\theta_l(r^\alpha_i=h, r^\beta_j=h, r^\gamma_k=h) - F^\theta_l(r^\alpha_i=h, r^\beta_j=h, r^\gamma_k=-h)\\
&- F^\theta_l(r^\alpha_i=h, r^\beta_j=-h, r^\gamma_k=h) + F^\theta_l(r^\alpha_i=h, r^\beta_j=-h, r^\gamma_k=-h)\\
&- F^\theta_l(r^\alpha_i=-h, r^\beta_j=h, r^\gamma_k=h) + F^\theta_l(r^\alpha_i=-h, r^\beta_j=h, r^\gamma_k=-h)\\
&+ F^\theta_l(r^\alpha_i=-h, r^\beta_j=-h, r^\gamma_k=h) - F^\theta_l(r^\alpha_i=-h, r^\beta_j=-h, r^\gamma_k=-h)\Big],
\end{aligned} \tag{11}$$

where h is a small displacement from the equilibrium position, and F^θ_l is the θ component of the force on the l-th atom. The default value of h is 0.04 times the Bohr radius, which can be changed by editing the header of the `Fourthorder.py` script. Each element of $\Phi^{\alpha\beta\gamma\theta}_{ijkl}$ requires eight DFT calculations with different supercell configurations, and there are $81n^4N^3$ elements a supercell with N unit cells with

n basis atoms per unit cell. A typical fourth-order IFCs calculation requires supercells containing more than 100 atoms, meaning that tens of thousands of single DFT simulation would be needed. Since directly performing these calculations is impractical for most computing infrastructures, it is crucial to make use of the symmetry analysis to reduce the computational cost.

We begin by populating the force constant matrices with transposition symmetries, and in the case of fourth-order IFCs this permutation of indices can have 24 sets of equality constraints

$$\Phi_{ijkl}^{\alpha\beta\gamma\theta} = \Phi_{ijlk}^{\alpha\beta\theta\gamma} = \dots \tag{12}$$

Then, we apply a space group symmetry operation $\sum_{\alpha} \mathbf{T}^{\alpha'\alpha}\mathbf{R}_i^{\alpha} + \mathbf{b}^{\alpha'} = \mathbf{R}_{\mathbf{T}_{b(i)}}^{\alpha'}$ to the tensor, where $\mathbf{T}$ and $\mathbf{b}$ represent the point-group and translation operators respectively, and $\mathbf{T}_{b(i)}$ specifies the atom to which the i-th atom is mapped under the corresponding operation. The fourth-order IFC tensor must satisfy the following relation:

$$\Phi_{\mathbf{T}_{b(i)};\mathbf{T}_{b(j)};\mathbf{T}_{b(k)};\mathbf{T}_{b(l)}}^{\alpha'\beta'\gamma'\theta'} = \sum_{\alpha\beta\gamma\theta} \mathbf{T}^{\alpha'\alpha}\mathbf{T}^{\beta'\beta}\mathbf{T}^{\gamma'\gamma}\mathbf{T}^{\theta'\theta}\Phi_{ijkl}^{\alpha\beta\gamma\theta}. \tag{13}$$

Each symmetry operation enables to map the four atom indices i, j, k, l into themselves or to a different set. The first class of operations enforces m constraints on the set of 81 fourth-order IFCs related to an atomic quartette, and each constraint can be described by a linear equation. Using Gaussian elimination, the m linear equations can be transformed into the following form:

$$\begin{pmatrix} 1 & 0 & * & 0 & 0 & \dots \\ 0 & 1 & * & 0 & 0 & \dots \\ 0 & 0 & 0 & 1 & 0 & \dots \\ 0 & 0 & 0 & 0 & 1 & \dots \\ \vdots & \vdots & \vdots & \vdots & \vdots & \vdots \end{pmatrix} \begin{pmatrix} x_1 \\ x_2 \\ x_3 \\ \vdots \\ x_{81} \end{pmatrix} = 0, \tag{14}$$

where asterisks in the columns stand for arbitrary numbers, corresponding to the independent elements among the set of 81 IFCs. The remaining force constants are linear combinations of them. Likewise with `thirdorder.py`, `Fourthorder.py` relies on the `spglib` library for detecting all kinds of crystal symmetries.

The fourth-order IFC tensor also obeys the acoustic sum rules (ASRs)

$$\sum_{l} \Phi_{ijkl}^{\alpha\beta\gamma\theta} = 0. \tag{15}$$

Considering transposition symmetries mentioned above, Eq. (15) must also be valid if the summation is performed over i, j, or k.

Whether these sums are exactly zero has a significant effect on the calculated phonon scattering rates at low frequencies near the $\mathbf{\Gamma}$ point. Numerical uncertainties usually lead to small violations in ASRs, leading to significant deviations in calculated scattering rates. To tackle this problem, we adopt the same method with `thirdorder.py` [12], namely adding a small compensation to each independent non-zero IFC, where the compensation is chosen by minimizing the sum of squares of these compensations by introducing a Lagrange multiplier.

It should also be noted that the fourth-order IFCs convergence with respect to the cutoff interatomic distance has to be checked manually, by examining either the force constants directly or the calculated thermal conductivity values. The computational cost increases significantly with increasing cutoff interatomic distance. Fortunately, it has been found [14,21,28–30] that, for many three-dimensional crystals, including up to the second-nearest neighbors in the fourth-order IFCs can give satisfactorily converged values of scattering rates and lattice thermal conductivity.

We note that the calculation of fourth-order IFCs is still computationally expensive using the above finite differences scheme. More efficient techniques are available, such as compressive sensing lattice dynamics (CSLD) [31] and a similar approach called hiPhive [32], for which open source codes have been developed. It is claimed that these methods can speed up the calculation while preserving accuracy to obtain reasonable results [33]. Other developments include using the moment tensor potential (MTP) to generate force constants [34,35]. These advancements can potentially benefit our users as one can use force constants from other software or methods. More tests can be done to check the applicability and accuracy of these methods on a wide range of materials.

2.4. Adaptive broadening for energy conservation

The delta function δ for energy conservation is approximated by using the adaptive Gaussian broadening method [36,37]. The expression for four-phonon processes is similar to three-phonon case. Energy spacing level is described by taking the derivative of energy difference respect to the third phonon involved $\frac{\partial\Delta\omega}{\partial\mathbf{q}''}$. This adaptive broadening then needs the group velocity of a certain mode $\mathbf{v}_{\lambda}$ and the spacing of sampling $\mathbf{q}$ points $|\Delta\mathbf{q}''|$. The formula is expressed as:

$$\delta(\omega_{\lambda} \pm \omega_{\lambda'} \pm \omega_{\lambda''} - \omega_{\lambda'''}) \approx \frac{1}{\sqrt{\pi}\sigma} e^{-\frac{(\Delta\omega)^2}{\sigma^2}}, \tag{16}$$

while the parameter σ for different processes is calculated as:

$$\sigma = |\mathbf{v}_{\lambda''} - \mathbf{v}_{\lambda'''}||\Delta\mathbf{q}''| \tag{17}$$

The detailed derivations for this formula can be found in Appendix B. Similar to `ShengBTE`, users of this program can always adopt a smaller `scalebroad` to reduce the computational cost by including fewer four-phonon processes, and it can often give reasonable results. Our implementation also addresses a technical problem. When σ evaluated is very small, the calculated scattering rates may be some abnormally high values. This numerical error is corrected by setting the δ function as 1.

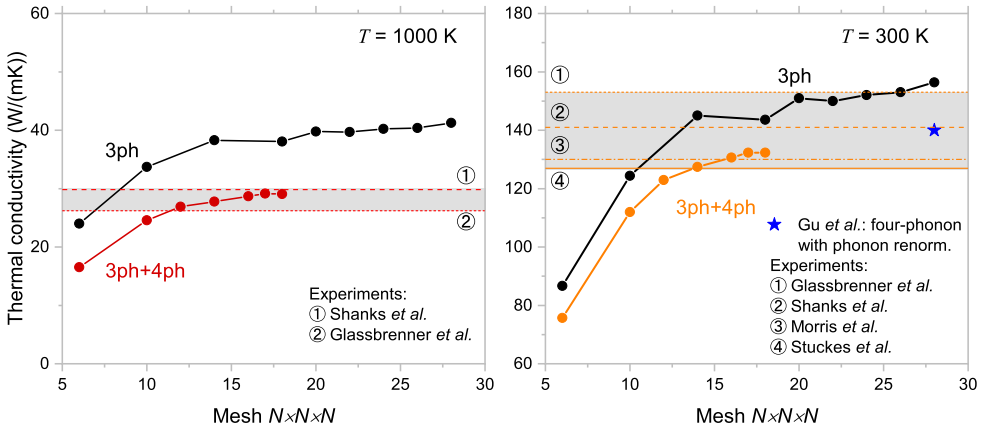

Fig. 2. Thermal conductivity of Si at 1000 K and 300 K calculated by `ShengBTE` with `FourPhonon` using first principles. The plot shows the convergence curve with respect of the **q**-points mesh. The value of *scalebroad* is taken as 0.1. Experimental data are represented by red straight lines for 1000 K (dot line [39], dash line [40]), and orange straight lines for 300 K (dot dash line [41], solid line [42], dash line [40], dot line [39]). The star in the right panel represents a recent theoretical work considering both four-phonon scattering and phonon renormalization [38]. They have used an extrapolation scheme for four-phonon scattering such that denser mesh is extrapolated with the scattering rates at mesh $N = 12$.

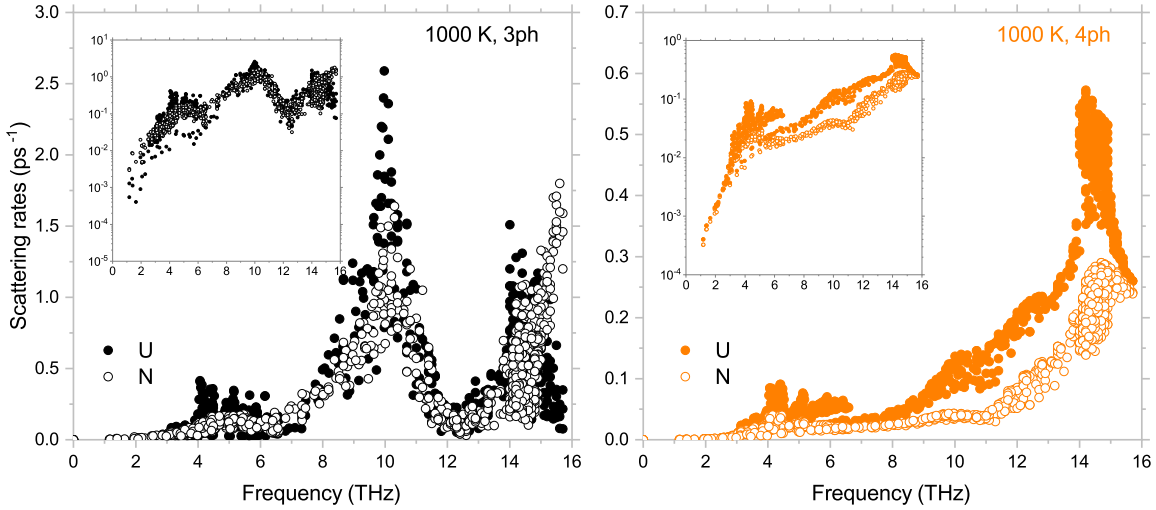

Fig. 3. Phonon scattering rates of Si at 1000 K (left: three-phonon, right: four-phonon). The value of *scalebroad* is taken as 0.1. The inset is log-scale in scattering rates. In both figures, solid circles indicate phonon Umklapp process while hollow ones represent normal process.

3. Examples

3.1. Si

Being the most commonly used semiconductor, silicon has been extensively studied as a benchmark material for theoretical predictions. We use silicon to illustrate the common practice for calculating thermal conductivity with four-phonon scattering.

Force constants are all calculated by first principles and are consistent with a previous study [14]. Using a $6 \times 6 \times 6$ supercell, we have considered up to the fifth-nearest neighboring atoms in the third-order IFCs and second-nearest neighboring atoms in the fourth-order IFCs. Calculation of these IFCs is nearly a standard process and is well documented in some helpful tutorials [11]. In the calculation of all three examples, we have turned on the iterative flag for three-phonon scattering.

Regarding the convergence with respect to the **q**-points, our tests on silicon show that (see Fig. 2) the inclusion of four-phonon scattering would only require a $17 \times 17 \times 17$ **q**-points grid to produce converged thermal conductivity values. In contrast, three-phonon scattering typically requires a $25 \times 25 \times 25$ **q**-points grid to converge. This is beneficial given the fact that the calculation of four-phonon scattering is very expensive. At 300 K, our results fall slightly lower than some experiments. This could be potentially remedied by considering phonon renormalization effect in the calculation. A recent study incorporating these effects reported room temperature thermal conductivity around 140 W/m·K [38], which is within the range of experimental uncertainty.

Details on phonon-phonon interactions in Si at 1000 K are shown in Fig. 3. Consistent with the literature [14], normal three-phonon processes do not overwhelm Umklapp processes. And in the four-phonon scattering, Umklapp process is dominant. Thus, applying only RTA scheme to Si is acceptable in calculating thermal conductivity.

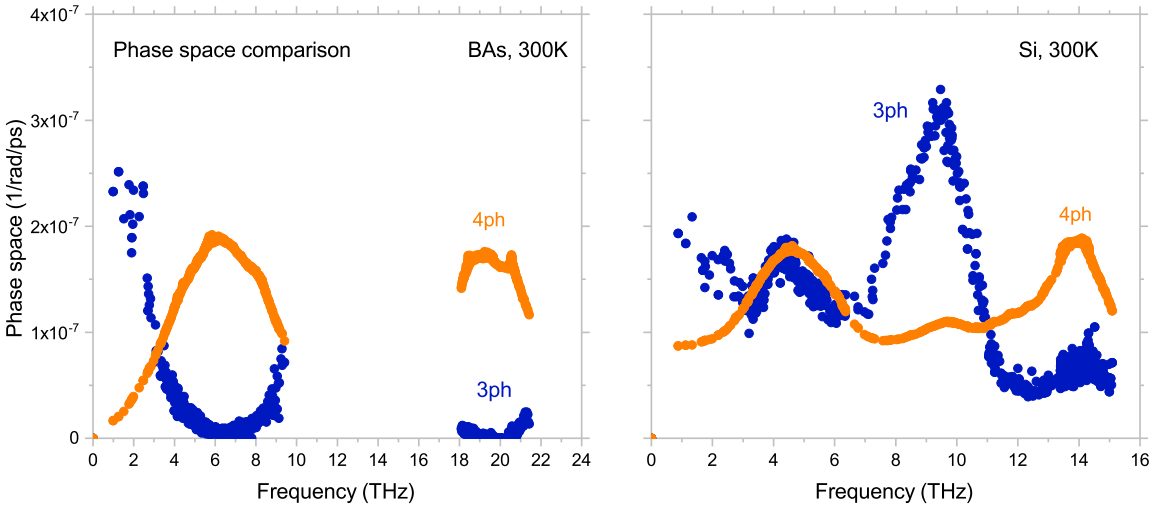

Fig. 4. Phase space available of BAs (left) and Si (right) at 300 K. The value of *scalebroad* is taken as 0.1 and data is presented in log-scale. In both figures, blue circles represent the phase space for three-phonon scattering events (P_3), and orange circles represent the phase space for four-phonon scattering events (P_4).

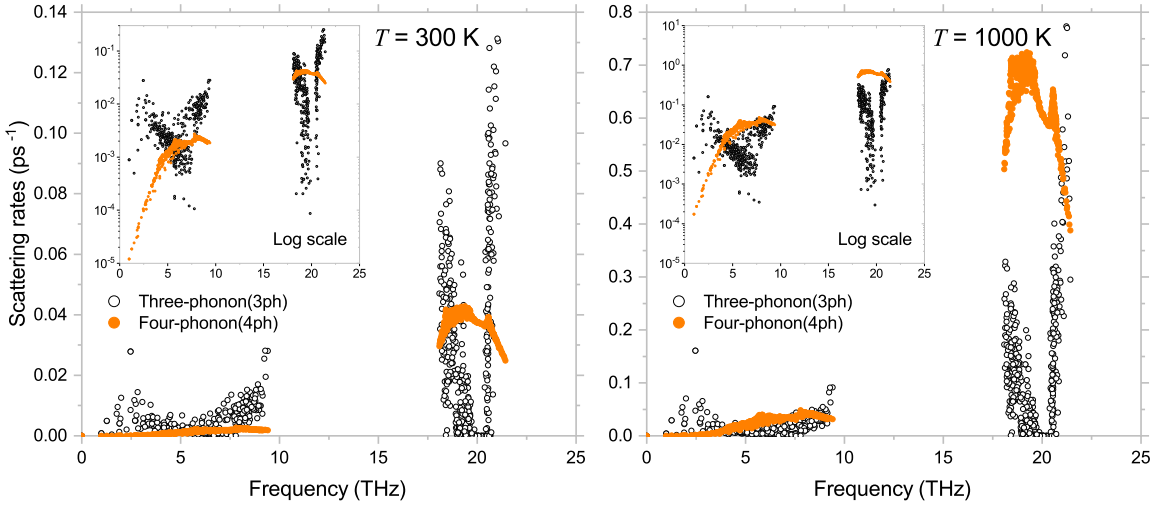

Fig. 5. Phonon scattering rates of BAs at 300 K (left) and 1000 K (right). The value of *scalebroad* is taken as 0.1. The inset is log-scale in scattering rates. One can observe from the logarithm scale that when frequency approaches zero, the scattering rate also goes down to zero, or $\lim_{\omega\to 0}\tau^{-1}=0$.

3.2. BAs

Four-phonon effect is known to be important in boron arsenide (BAs), a zinc-blende structure material promising for thermal management applications. When determining the intrinsic thermal transport process, four-phonon scattering is even stronger than three-phonon scattering. It was found that the higher-order anharmonicity would result in a substantial reduction of thermal conductivity [14], and subsequent experimental studies [15–17] have validated the predicted thermal conductivity values. Therefore, we use BAs as an example material to further illustrate `FourPhonon` workflow in calculating thermal conductivity.

The sets of IFCs are obtained from first principles on a $4\times4\times4$ supercell. Following parameters used in the literature, we firstly perform calculations on a $16\times16\times16$ **q**-points grid with `scalebroad`=0.1 at 300 K. For illustrating purpose, we assume that at this stage users have no knowledge on how important four-phonon effect is in BAs. Instead of directly calculating scattering rates with potentially very high cost, one can first look at the weighted phase space as defined in Ref. [43]. This is done by turning on `onlyharmonic` and `four_phonon` flags in the `CONTROL` file. Phase space calculation is less expensive to perform since it does not involve anharmonic IFCs. The results are shown in Fig. 4. We also plot the results of Si for comparison. It is found that phase space of four-phonon scattering is quite large in BAs, especially in optical branches. In contrast, in Si, four-phonon phase space is generally smaller than three-phonon phase space. This is consistent with the fact that four-phonon scattering is not significant in silicon at room temperature and only has minor effect on its thermal conductivity [14]. Thus, the calculation of phase space can provide a preliminary estimation if four-phonon scattering needs to be considered for thermal transport study or not.

Fig. 5 presents the phonon scattering rates in BAs at 300 K and 1000 K. The four-phonon scattering rates can be comparable to or even larger than three-phonon ones even at room temperature. The scattering rates calculation takes about 1680 CPU hours for a single temperature point. For the benefit of our users, the actual computational costs of tasks performed in this paper are summarized in Appendix C.

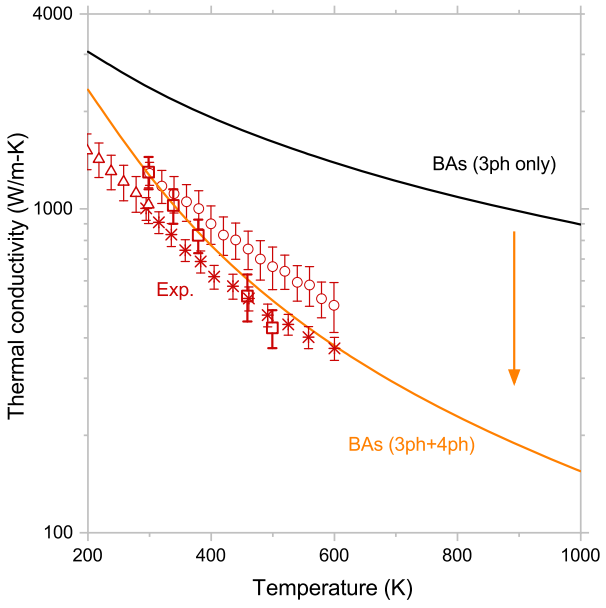

Fig. 6. Thermal conductivity of naturally occurring BAs. The value of *scalebroad* is taken as 0.1. Red symbols are from three experimental works. Red triangle and red square are from Ref. [16], red circles Ref. [15], red stars Ref. [17].

Thermal conductivity is then obtained by exactly solving BTE in an iterative scheme involving three-phonon interactions. To ensure the accuracy of `scalebroad`, we also perform calculations on the same mesh with `scalebroad`=1. The thermal conductivity values in W/m·K are 1221.9 (`scalebroad`=1) vs. 1266.9 (`scalebroad`=0.1), and the relative difference is within 4%. Considering the fact that four-phonon scattering calculations are very expensive at a larger broadening factor, we set `scalebroad`=0.1 in calculations at all temperature points. Note that room temperature thermal conductivity predicted in Ref. [16] using fully iterative solution of BTE and tetrahedron scheme is 1260 W/m·K, which is very close to our result. This confirms that in BAs Umklapp process is still dominant in four-phonon scattering [14].

After performing calculations from 200 K to 1000 K, we get the temperature-dependent thermal conductivity, as shown in Fig. 6. Consistent with results in Fig. 5, larger reductions are observed for higher temperatures when considering four-phonon scattering. Our results are in good agreement with experimental data.

3.3. $LiCoO_2$

$LiCoO_2$ is a representative material of layered lithium transition-metal oxides (Li_xTMO_2). This family of materials store lithium ions in between the TMO_2 layers, and have significant applications in rechargeable batteries due to their superior electrical and mechanical properties. However, their thermal transport properties seem to be hindering the improvement of device performance [30,44]. As revealed by Feng et al. [30], the theoretical upper limit of $LiCoO_2$'s lattice thermal conductivity would be lowered 2-6 times when including higher-order lattice anharmonicity. Compared to the preceding examples, lithium transition-metal oxides have more complex structures and involve four atoms in the unit cell. In this part, we intend to calculate the thermal transport properties of $LiCoO_2$ using our new computational tool, and decompose the scattering rates into different scattering channels (i.e., recombination, redistribution and splitting processes).

A $3 \times 3 \times 3$ supercell is employed to obtain IFCs by first principles (for detailed information see Ref. [30]) and the Brillouin zone is discretized by $10 \times 10 \times 10$ $\mathbf{q}$-points grid. For this material with complex lattice structures, we only use `scalebroad`=0.01 to perform four-phonon calculations, and the available four-phonon processes are already around 10^{10}.

Results of phonon scattering rates are shown in Fig. 7. Even at room temperature, four-phonon scattering rates of $LiCoO_2$ are generally comparable to three-phonon scattering rates over the entire frequency range. Different from BAs, four-phonon scattering rates are not that significant in optical phonon branches. Decomposing the four-phonon interactions further into different scattering channels provides us with more information. One can observe that redistribution process ($\lambda + \lambda' \rightarrow \lambda'' + \lambda'''$) contributes the most and Umklapp process dominates this specific scattering channel.

We then calculate the in-plane ($\kappa_\parallel$) and through-plane ($\kappa_\perp$) thermal conductivity and compare their values with the literature. Such information is available in a file named `BTE.kappa_tensor`. At 300 K, our calculations yield 9.35 W/m·K for $\kappa_\parallel$ and 1.39 W/m·K for $\kappa_\perp$, which agree reasonably well with Ref. [30] that gives 9.7 W/m·K and 1.4 W/m·K, respectively.

4. Conclusion

The recent introduction and implementation of Feng and Ruan's four-phonon calculation framework has led the community to revise the understanding of thermal transport theory. This motivated us to develop a computational package, `FourPhonon`, that can make this calculation accessible to the thermal science community and enable researchers to explore four-phonon effects in a broader range of topics. This new program is developed under a well-perceived phonon calculation platform `ShengBTE`. Our main contribution is:

- Provide the first open-source tool to perform four-phonon scattering calculations, while preserve nice features of `ShengBTE` platform;

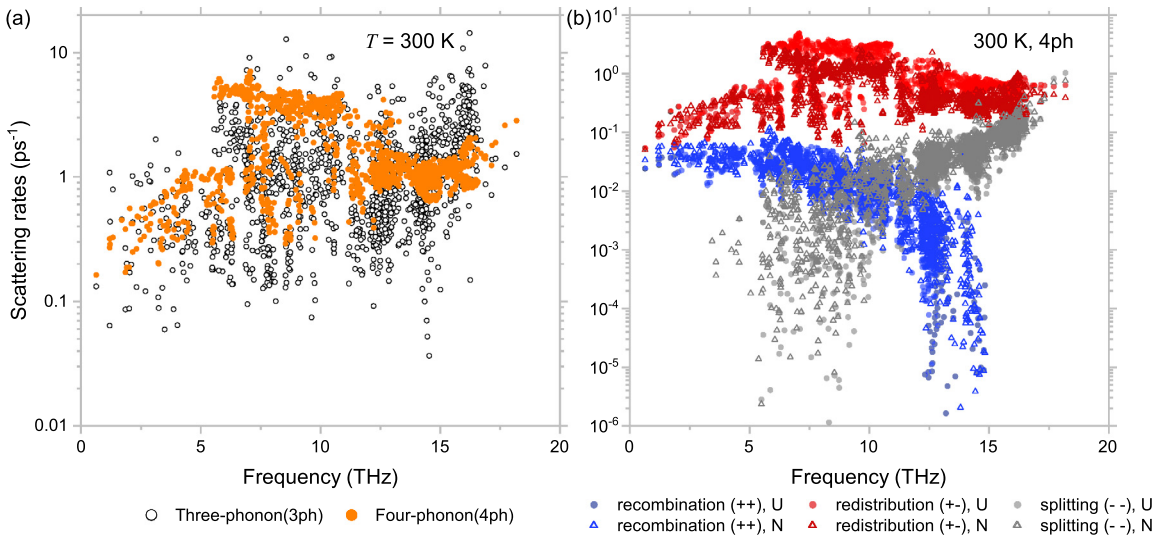

Fig. 7. Phonon scattering rates of $LiCoO_2$ at 300 K. In both figures, scalebroad = 0.01 and y-axis is presented in logarithm scale. Figure (a) shows the comparative strength of three- and four-phonon scattering rates. Captions in (b) represent scattering rates from three scattering channels: recombination ($\lambda + \lambda' + \lambda'' \rightarrow \lambda'''$), redistribution ($\lambda + \lambda' \rightarrow \lambda'' + \lambda'''$) and splitting ($\lambda \rightarrow \lambda' + \lambda'' + \lambda'''$).

- Extend the adaptive broadening scheme to four-phonon scattering cases, provide a script for fourth-order force constants calculations that utilizes both the point-group and translational symmetries.

Examples on silicon, BAs and $LiCoO_2$ cover common materials, typical materials known for significant four-phonon effects, and newly reported complex systems. These examples show different aspects of our new program and some technical features like convergence with respect to broadening factor and **q**-points grid, scattering contributions from Umklapp and normal processes or from different scattering channels.

Our program is currently able to perform four-phonon calculations under Single Mode Relaxation Time Approximation and iterate with three-phonon scattering rates. We look forward to providing the community with a version capable of fully four-phonon iterative calculations when the memory issue is resolved.

Declaration of competing interest

The authors declare that they have no known competing financial interests or personal relationships that could have appeared to influence the work reported in this paper.

Acknowledgements

X. R. and Z. H. acknowledge the partial support from the National Science Foundation (Grant No. 2015946). Simulations were performed at the Rosen Center for Advanced Computing (RCAC) of Purdue University. X. Y. acknowledges support from the Natural Science Foundation of China (Grant No. 12004254). W. L. acknowledges support from the GuangDong Basic and Applied Basic Research Foundation (Grant No. 2021A1515010042) and the Stable Support Plan of the Higher Education Institutions of Shenzhen (Grant No. 20200809161605001). We thank Dr. Lucas Lindsay for providing force constants of Si, as reported in Ref. [14].

Appendix A. Input and output files of `FourPhonon`

Apart from the input files required by `ShengBTE`, `FourPhonon` takes an additional force constants file, namely `FORCE_CONSTANTS_4TH`. This file can be generated using our script `Fourthorder.py`. Consistent with `ShengBTE`, our program takes no command-line arguments and users only need to prepare a `CONTROL` file that contains all the settings on crystal structures, energy broadening factor, and **q**-points grid. To enable the four-phonon calculations, users should set `four_phonon=.TRUE.` in this file. After the computations, we will have these output files besides normal outputs from `ShengBTE`:

`BTE.Numprocess_4ph`:	number of allowed four-phonon scattering processes for each mode.
`BTE.P4`:	phase space available for four-phonon scatterings.
`BTE.WP4`:	weighted phase space available for four-phonon processes.
`BTE.w_4ph`:	four-phonon scattering rates under RTA.
`BTE.w_4ph_Umklapp`:	four-phonon scattering rates from Umklapp processes under RTA.
`BTE.w_4ph_normal`:	four-phonon scattering rates from normal processes under RTA.

Appendix B. Derivation of adaptive broadening formulas

For a certain phonon mode $(\mathbf{q}, \omega)$, the other three phonons involved are located $\mathbf{q}', \mathbf{q}'', \mathbf{q}'''$ in k-space and their corresponding frequencies are $\omega', \omega'', \omega'''$. The fourth phonon $(\mathbf{q}''', \omega''')$ is dependent on the choice of the second and the third phonon while the second phonon $(\mathbf{q}', \omega')$ and the third phonon $(\mathbf{q}'', \omega'')$ are independent from each other. Energy spacing level can be expressed for different scattering processes and then take the derivative:

For recombination (++) process, $\Delta\omega = -\omega' - \omega'' + \omega'''$ and $\mathbf{q} + \mathbf{q}' + \mathbf{q}'' = \mathbf{q}'''$, we have

$$\frac{\partial \Delta\omega}{\partial \mathbf{q}''} = -\frac{\partial \omega''}{\partial \mathbf{q}''} + \frac{\partial \omega'''}{\partial \mathbf{q}'''}\frac{\partial \mathbf{q}'''}{\partial \mathbf{q}''} = -\mathbf{v}_{\lambda''} + \mathbf{v}_{\lambda'''} \tag{B.1}$$

for redistribution (+ -) process, $\Delta\omega = -\omega' + \omega'' + \omega'''$ and $\mathbf{q} + \mathbf{q}' - \mathbf{q}'' = \mathbf{q}'''$, we have

$$\frac{\partial \Delta\omega}{\partial \mathbf{q}''} = \frac{\partial \omega''}{\partial \mathbf{q}''} + \frac{\partial \omega'''}{\partial \mathbf{q}'''}\frac{\partial \mathbf{q}'''}{\partial \mathbf{q}''} = \mathbf{v}_{\lambda''} + \mathbf{v}_{\lambda'''}(-1) \tag{B.2}$$

for splitting (- -) process, $\Delta\omega = \omega' + \omega'' + \omega'''$ and $\mathbf{q} - \mathbf{q}' - \mathbf{q}'' = \mathbf{q}'''$, we have

$$\frac{\partial \Delta\omega}{\partial \mathbf{q}''} = \frac{\partial \omega''}{\partial \mathbf{q}''} + \frac{\partial \omega'''}{\partial \mathbf{q}'''}\frac{\partial \mathbf{q}'''}{\partial \mathbf{q}''} = \mathbf{v}_{\lambda''} + \mathbf{v}_{\lambda'''}(-1) \tag{B.3}$$

energy broadening factor $\sigma = |\frac{\partial \Delta\omega}{\partial \mathbf{q}''}||\Delta\mathbf{q}''|$ then yields

$$\sigma = \begin{cases} |-\mathbf{v}_{\lambda''} + \mathbf{v}_{\lambda'''}||\Delta\mathbf{q}''|, & \text{for recombination (++) process} \\ |\mathbf{v}_{\lambda''} - \mathbf{v}_{\lambda'''}||\Delta\mathbf{q}''|, & \text{for redistribution (+ -) process} \\ |\mathbf{v}_{\lambda''} - \mathbf{v}_{\lambda'''}||\Delta\mathbf{q}''|, & \text{for splitting (- -) process.} \end{cases} \tag{B.4}$$

Since we are taking the absolute value, the final formula for all the processes is then

$$\sigma = |\mathbf{v}_{\lambda''} - \mathbf{v}_{\lambda'''}||\Delta\mathbf{q}''| \tag{B.5}$$

Appendix C. Computational costs of `FourPhonon`

All calculations are done at the Rosen Center for Advanced Computing (RCAC) at Purdue University. The cluster is equipped with Sky Lake CPUs that have a clock frequency of 2.60 GHz. Here we report the computational costs in terms of CPU hours which include a single temperature point calculation using `FourPhonon` to calculate scattering rates and thermal conductivity. The data are presented below in Tables C.1, C.2 and C.3 (σ is the broadening factor):

Table C.1
CPU hours spent in the calculations on Si.

Mesh size ($N \times N \times N$)	Broadening factor	
	$\sigma = 0.1$	$\sigma = 1$
10	24	192
16	990	6912
18	4992	16896

Table C.2
CPU hours spent in the calculations on BAs.

Mesh size ($N \times N \times N$)	Broadening factor	
	$\sigma = 0.1$	$\sigma = 1$
16	1680	7488

Table C.3
CPU hours spent in the calculations on $LiCoO_2$.

Mesh size ($N \times N \times N$)	Broadening factor	
	$\sigma = 0.01$	$\sigma = 0.1$
10	360	2800
11	864	6408

References

[1] R. Peierls, Ann. Phys. 395 (8) (1929) 1055–1101.
[2] J. Callaway, Phys. Rev. 113 (4) (1959) 1046.
[3] J.M. Ziman, in: International Series of Monographs on Physics, (Oxford, England), Clarendon Press, Oxford, 1960.
[4] A.A. Maradudin, A.E. Fein, Phys. Rev. 128 (6) (1962) 2589–2608, https://doi.org/10.1103/physrev.128.2589.
[5] M. Omini, A. Sparavigna, Physica B, Condens. Matter 212 (2) (1995) 101–112.
[6] D.A. Broido, M. Malorny, G. Birner, N. Mingo, D. Stewart, Appl. Phys. Lett. 91 (23) (2007) 231922.
[7] K. Esfarjani, G. Chen, H.T. Stokes, Phys. Rev. B 84 (8) (2011) 085204, https://doi.org/10.1103/physrevb.84.085204, arXiv:1107.5288.
[8] L. Lindsay, D. Broido, T. Reinecke, Phys. Rev. Lett. 111 (2) (2013) 025901.
[9] A. Seko, A. Togo, H. Hayashi, K. Tsuda, L. Chaput, I. Tanaka, Phys. Rev. Lett. 115 (20) (2015) 205901.
[10] L. Lindsay, C. Hua, X. Ruan, S. Lee, Proc. Natl. Acad. Sci. 114 (2017), Mater. Today Phys. 7 (2018) 106–120, https://doi.org/10.1016/j.mtphys.2018.11.008.
[11] A.J.H. McGaughey, A. Jain, H.-Y. Kim, J. Appl. Phys. 125 (1) (2019) 011101, https://doi.org/10.1063/1.5064602.

[12] W. Li, J. Carrete, N.A. Katcho, N. Mingo, Comput. Phys. Commun. 185 (6) (2014) 1747–1758.
[13] T. Feng, X. Ruan, Phys. Rev. B 93 (4) (2016) 045202, https://doi.org/10.1103/physrevb.93.045202.
[14] T. Feng, L. Lindsay, X. Ruan, Phys. Rev. B 96 (16) (2017) 161201, https://doi.org/10.1103/physrevb.96.161201.
[15] J.S. Kang, M. Li, H. Wu, H. Nguyen, Y. Hu, Science 361 (6402) (2018) 575–578, https://doi.org/10.1126/science.aat5522.
[16] F. Tian, B. Song, X. Chen, N.K. Ravichandran, Y. Lv, K. Chen, S. Sullivan, J. Kim, Y. Zhou, T.-H. Liu, M. Goni, Z. Ding, J. Sun, G.A.G.U. Gamage, H. Sun, H. Ziyaee, S. Huyan, L. Deng, J. Zhou, A.J. Schmidt, S. Chen, C.-W. Chu, P.Y. Huang, D. Broido, L. Shi, G. Chen, Z. Ren, Science 361 (6402) (2018) 582–585, https://doi.org/10.1126/science.aat7932.
[17] S. Li, Q. Zheng, Y. Lv, X. Liu, X. Wang, P.Y. Huang, D.G. Cahill, B. Lv, Science 361 (6402) (2018) 579–581, https://doi.org/10.1126/science.aat8982.
[18] T. Feng, X. Ruan, Phys. Rev. B 97 (4) (2018) 045202, https://doi.org/10.1103/physrevb.97.045202.
[19] Y. Xia, M.K.Y. Chan, Appl. Phys. Lett. 113 (19) (2018) 193902, https://doi.org/10.1063/1.5048814.
[20] N.K. Ravichandran, D. Broido, Phys. Rev. B 98 (8) (2018) 085205, https://doi.org/10.1103/physrevb.98.085205.
[21] X. Yang, T. Feng, J.S. Kang, Y. Hu, J. Li, X. Ruan, Phys. Rev. B 101 (16) (2020) 161202, https://doi.org/10.1103/physrevb.101.161202.
[22] N.K. Ravichandran, D. Broido, Phys. Rev. X 10 (2) (2020) 021063, https://doi.org/10.1103/physrevx.10.021063, arXiv:2003.08893.
[23] A. Kundu, X. Yang, J. Ma, T. Feng, J. Carrete, X. Ruan, G.K. Madsen, W. Li, Phys. Rev. Lett. 126 (11) (2021) 115901.
[24] T. Feng, X. Ruan, in: Nanoscale Energy Transport, 2053-2563, IOP Publishing, 2020 pp. 2–1 to 2–44, http://dx.doi.org/10.1088/978-0-7503-1738-2ch2.
[25] L. Lindsay, D. Broido, N. Mingo, Phys. Rev. B 82 (11) (2010) 115427.
[26] A. Maradudin, A. Fein, Phys. Rev. 128 (6) (1962) 2589.
[27] T. Tadano, Y. Gohda, S. Tsuneyuki, J. Phys. Condens. Matter 26 (22) (2014) 225402.
[28] X. Yang, T. Feng, J. Li, X. Ruan, Phys. Rev. B 100 (24) (2019) 245203.
[29] Z. Tong, X. Yang, T. Feng, H. Bao, X. Ruan, Phys. Rev. B 101 (12) (2020) 125416.
[30] T. Feng, A. O'Hara, S.T. Pantelides, Nano Energy (2020) 104916.
[31] F. Zhou, W. Nielson, Y. Xia, V. Ozoliņš, Phys. Rev. Lett. 113 (18) (2014) 185501, https://doi.org/10.1103/physrevlett.113.185501.
[32] F. Eriksson, E. Fransson, P. Erhart, Adv. Theory Simul. 2 (5) (2019) 1800184.
[33] Y. Xia, V.I. Hegde, K. Pal, X. Hua, D. Gaines, S. Patel, J. He, M. Aykol, C. Wolverton, Phys. Rev. X 10 (4) (2020) 041029, https://doi.org/10.1103/physrevx.10.041029.
[34] A.V. Shapeev, Multiscale Model. Simul. 14 (3) (2016) 1153–1173.
[35] B. Mortazavi, E.V. Podryabinkin, I.S. Novikov, T. Rabczuk, X. Zhuang, A.V. Shapeev, Comput. Phys. Commun. 258 (2021) 107583, https://doi.org/10.1016/j.cpc.2020.107583.
[36] W. Li, N. Mingo, L. Lindsay, D.A. Broido, D.A. Stewart, N.A. Katcho, Phys. Rev. B 85 (19) (2012) 195436, https://doi.org/10.1103/physrevb.85.195436.
[37] J.R. Yates, X. Wang, D. Vanderbilt, I. Souza, Phys. Rev. B 75 (19) (2007) 195121, https://doi.org/10.1103/physrevb.75.195121.
[38] X. Gu, S. Li, H. Bao, Int. J. Heat Mass Transf. 160 (2020) 120165.
[39] C.J. Glassbrenner, G.A. Slack, Phys. Rev. 134 (4A) (1964) A1058.
[40] H. Shanks, P. Maycock, P. Sidles, G. Danielson, Phys. Rev. 130 (5) (1963) 1743.
[41] R.G. Morris, J.G. Hust, Phys. Rev. 124 (5) (1961) 1426.
[42] A.D. Stuckes, Philos. Mag. 5 (49) (1960) 84–99.
[43] W. Li, N. Mingo, Phys. Rev. B 91 (14) (2015) 144304.
[44] K. Liu, Y. Liu, D. Lin, A. Pei, Y. Cui, Sci. Adv. 4 (6) (2018) eaas9820.